

# Flow patterns for an annular flow over an axisymmetric sudden expansion

By H. J. SHEEN, W. J. CHEN AND J. S. WU

Institute of Applied Mechanics, National Taiwan University, Taipei 10764, Taiwan  
*e-mail*: sheenh@spring.iam.ntu.edu.tw

(Received 21 November 1995 and in revised form 16 June 1997)

In this paper, an experimental investigation is described for a concentric annular flow over an axisymmetric sudden expansion by using both flow visualization and laser-Doppler anemometry (LDA) techniques. Depending upon the value of the Reynolds number and whether the Reynolds number was increased or decreased, four typical flow patterns were classified according to the characteristics of the central and corner recirculation zones. The flow patterns are open annular flow, closed annular flow, vortex shedding, and stable central flow. Bifurcation for this flow occurred when  $230 < Re < 440$ , which was verified by observing the variation of the reattachment length. The spatial growth of velocity fluctuations from the measurements demonstrated a tendency that shedding vortices behind the centrebody more strongly affect the reattachment length than flows without a centrebody.

---

## 1. Introduction and literature survey

An annular flow in a sudden-expansion circular channel is characterized by two reversed flow regions: the corner recirculation zone and the central recirculation zone. Both recirculation zones result from flow separation due to the abrupt changes of the boundary geometry introduced by the sudden-expansion step and the centrebody.

For an axisymmetric sudden-expansion flow without a centrebody, the reattachment length increases with the Reynolds number when, at relatively low Reynolds numbers, the flow is laminar. The variation of the reattachment length in an axisymmetric sudden-expansion pipe is almost linear as described by Macagno & Hung (1967) and Badekas & Knight (1992). For a plane-symmetric sudden-expansion flow at low Reynolds numbers, Durst, Pereira & Tropea (1993) found a symmetry-breaking bifurcation, which resulted in one long and one short separation zone for Reynolds numbers above 125. When the Reynolds number was increased above this critical value, the length of the short separated region remained nearly constant, but that of the long region increased. Armaly *et al.* (1983) investigated a flow over a single backward-facing step which was mounted in a two-dimensional channel. They indicated that the increase of the reattachment length at lower Reynolds numbers was not linear for this flow as reported by Macagno & Hung (1967) for the pipe expansion flow. They also mentioned that this was due to the difference in the configuration. The results of previous studies on higher-Reynolds-number turbulent flows, e.g. by Gould, Stevenson & Thompson (1990), Restivo & Whitelaw (1978) and Roos & Kegelmann (1986), showed that the reattachment lengths were slightly influenced by either the Reynolds number or the expansion ratio.

When the Reynolds number increases from the laminar flow regime but is still in

the intermediate regime, the reattachment location first reaches a maximum and then decreases to merge eventually with that for the higher Reynolds number turbulent flow. The evidence of a transitional regime reported by Armaly *et al.* (1983) in a single backward-facing step flow has been documented firstly by a sharp decrease of the reattachment length to a minimum value, and then an increase to a constant value which characterizes the turbulent flow regime. Eaton & Johnston (1981) also had similar results. For flow reattachments in axisymmetric sudden-expansion flows, Back & Roschke (1972) revealed that the existence of flow instabilities and coherent vortical structures, which developed in the shear layer, played an important role. Moreover, Roos & Kegelman (1986) showed that two-dimensional vortical structures, which formed in the reattaching shear layer, were generated in a flow over a single backward-facing step. With active forcing, the reattachment lengths could be substantially reduced. Regarding the effects of the centrebody in an annular jet, Chan & Ko (1978) studied annular jet flows and found that the presence of the central recirculation zone and the wake vortices behind the centrebody had the effect of accelerating the annular jet into a fully developed state. Ko & Chan (1979) mentioned that the flow fields within and near the internal recirculation region were dominated by the standing vortices and their propagation downstream.

In this investigation, the characteristic flow patterns are classified, and the corresponding reattachment lengths are quantitatively measured by using a flow visualization technique. Smoke patterns in the regions of the central recirculation zone and downstream were recorded to provide the pictures of various flow structures. A non-perturbative laser-Doppler anemometer was used to examine the spatial features of the velocity field and to verify the results by visual observations. Measurements of velocity fluctuations provided further evidence to justify the dominant mechanism of flow reattachment.

## 2. Experimental description

In this experiment, the air stream from two 11 KW air compressors passed through a dehumidifier filter into a 3.5 m<sup>3</sup> storage tank. The tank was used to ensure a regulated and stable air supply. An air filter and a pressure regulation valve placed at the outlet of the tank were used to clean and control the air flow. A vortex flow meter for higher flow rate and a rotameter for lower flow rate measurements were placed at the outlet of the storage tank to monitor the air flow. The air flow entered a settling chamber, which contained a honeycomb and two layers of screens in order to reduce the turbulence level. The flow then went through an axisymmetric contraction and finally entered the concentric annulus. The annular flow region had an inner diameter,  $d$ , of 21.7 mm, an outer diameter,  $D$ , of 45.3 mm, and a length of 200 mm. For the free-boundary case, in order to minimize the possible influence of draughts without affecting the entrainment of the surrounding air, the test region was surrounded by a cage 2 m  $\times$  2 m  $\times$  3 m with 0.8 mm meshes. For the confined-boundary case, a sudden-expansion Plexiglas tube with an inner diameter,  $D_o$ , of 90 mm was placed at the exit of the annulus. The test section had a step height,  $H$ , of 22.35 mm, and had a length of 1.2 m. The diameter expansion ratio,  $D_o/D$ , for the sudden expansion was 1.987. Figure 1 shows a schematic diagram of the experimental set-up and the test section.

Various flow patterns for the central and corner recirculation zones as well as the dynamic flow behaviours of vortex shedding were observed by using smoke streaks. Two methods were applied. For the central recirculation zone, a custom-

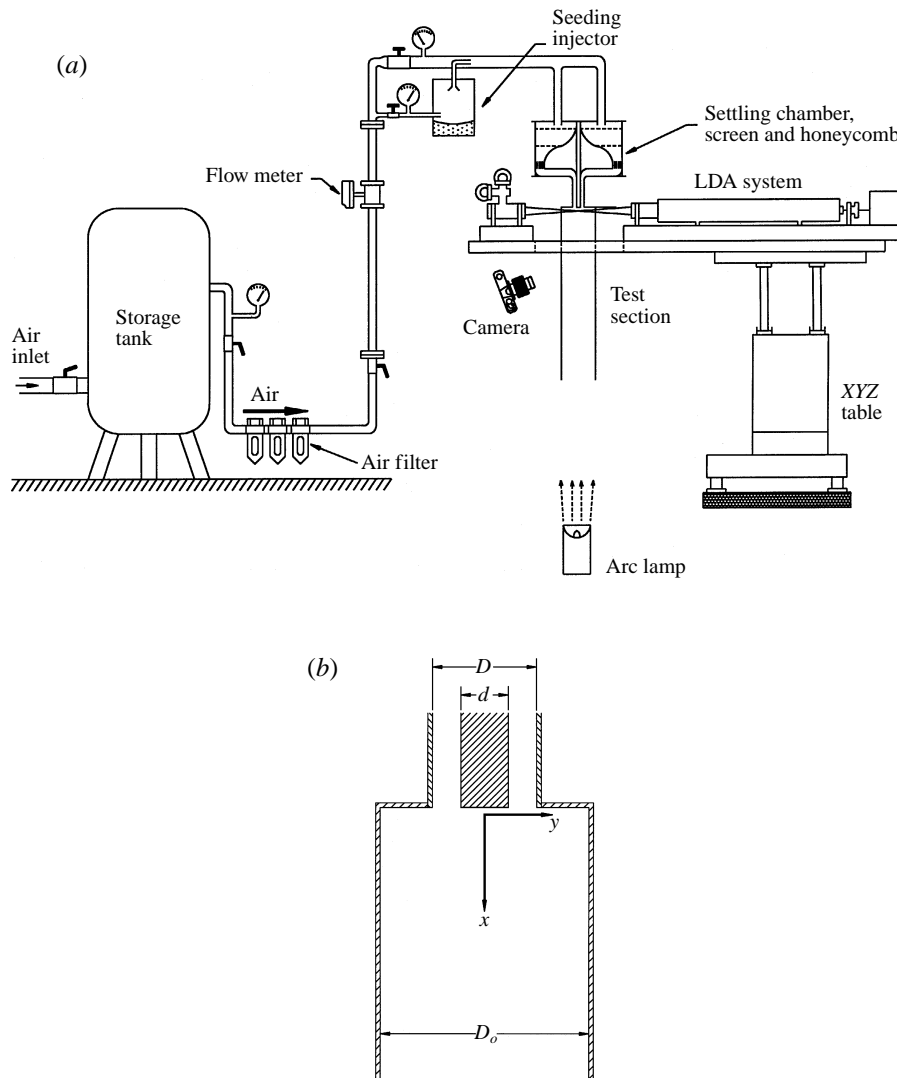


FIGURE 1. (a) Schematic diagram of the experimental set-up. (b) Coordinate system and dimensional symbols of the test section.

made miniature smoke generator was embedded inside the centreboby to vaporize the hydrocarbon oil. The vaporized smoke was then released from a very narrow slit at the base of the centreboby. The slightly sub-atmospheric pressure behind the centreboby provided a natural mechanism by which the dense smoke could be injected slowly to avoid disturbing the flow. To eliminate the possible error from the buoyancy effect, the power supply of the smoke generator was turned off after the smoke was generated. The smoke remained observable within the central recirculation zone for at least 30 s. Thereafter, the flow field illuminated by a 100 W arc-lamp was photographed with a Nikon F4 camera. The shutter speed of the camera was set at below 2 ms. In addition, a laser sheet, obtained by using a 3 W argon-ion laser and a cylindrical mirror, was applied to provide detailed images of the dynamic structures

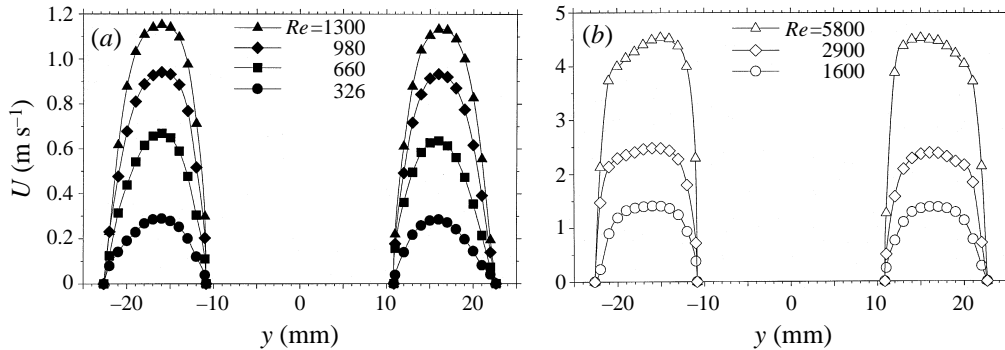


FIGURE 2. LDA measurements of the mean axial velocity profiles at the exit of the annular region with  $x/D_o=0.08$ , for (a) laminar flow regime; (b) transitional and turbulent flow regimes.

of the flow field. A Sony VX1 video camera was also used to observe the transient phenomena of the flow.

For the corner recirculation zone, the smoke injection method was applied. Cigarette smoke was injected into the corner recirculation region from one end of an L-shaped stainless steel tube with an OD of 1 mm. The other end of the stainless steel tube was connected to a syringe. The syringe was pushed by a stepping motor so that a very small amount of smoke was steadily injected into the corner recirculation region. By observing the direction in which the smoke streaks moved toward the step or downstream, the reattachment points could be determined. The flow rate of the smoke flow was adjusted to be less than 0.1% of the main flow.

A two-component forward-scattering laser-Doppler anemometry (LDA) (Tsi 9100-7) system was employed to carry out the velocity measurements. A 3 W argon-ion laser was used as the light source. The beam spacing was 50 mm, and the focusing length was 350 mm. Bragg cells were used for both components for the reversed flow measurements. A 2.27X beam expander was used to reduce the measuring volume and to increase the signal-to-noise ratio. Two counter-type signal processors with a DMA interface linked to a personal computer were used for data acquisition. Glass beads with nominal diameters of about  $1\ \mu\text{m}$  were used as the seeding tracer of the fluid phase for LDA measurements. The relaxation time for the tracer particles was estimated to be less than  $4\ \mu\text{s}$ . Glass beads were stored in a small tank and were carried out by the air flow through a cyclone. The LDA system was mounted on a computer-controlled X-Y-Z traversing system for measurement position adjustment. The precision of the traversing system was  $25\ \mu\text{m}$  for the Y- and Z-axes, and  $2.5\ \mu\text{m}$  for the X-axis. In this experiment, the uncertainties in LDA velocity measurements were estimated to be less than 3%.

LDA measurements of the velocity distributions at the test section inlet of the annular flow were carried out for Reynolds numbers ranging from 150 to 5800, which covered laminar, transitional and turbulent flow regimes. The Reynolds number was defined as

$$Re = \frac{U_m D_h}{\nu},$$

where  $U_m$  is the volumetric-mean axial velocity,  $D_h$  is the hydraulic diameter of the annular pipe,  $D_h = D - d$ ,  $D$  and  $d$  are the outer and inner diameters of the annulus, respectively, and  $\nu$  is the kinematic viscosity of air. Figure 2 shows a series of measured axial velocity profiles at the exit of the annular region with  $x/D = 0.08$ .

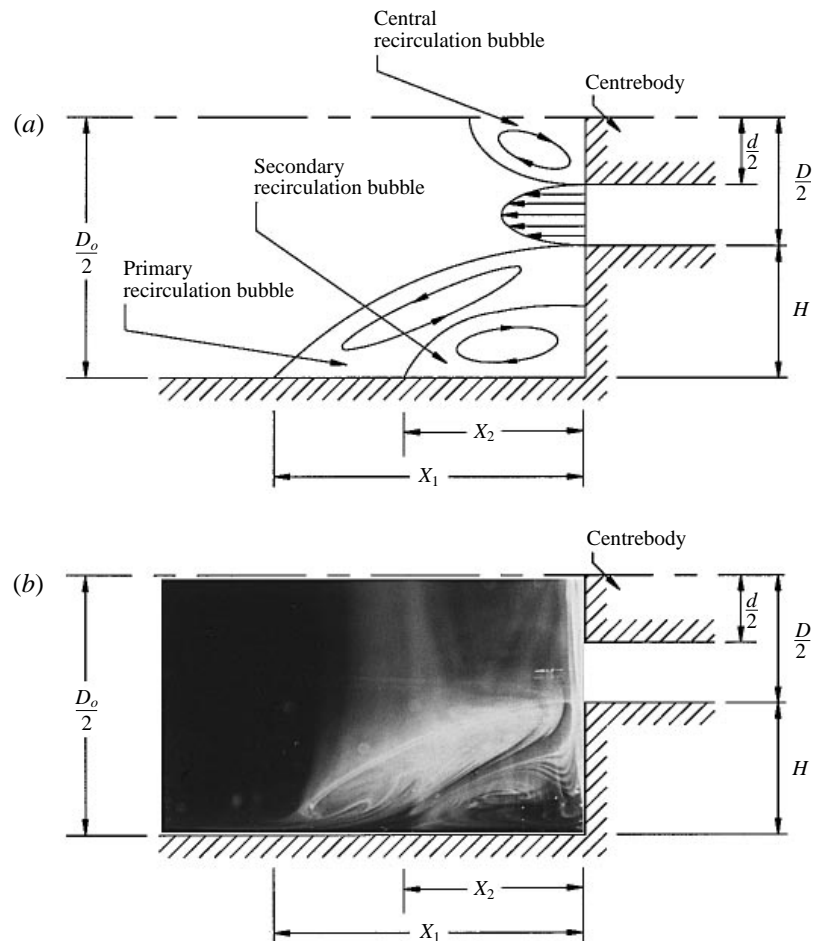


FIGURE 3. Recirculation zones of an annular flow over an axisymmetric sudden expansion: (a) schematic diagram; (b) photograph.

The results revealed that the annular flow at the annulus exit was axisymmetric in the laminar, transitional, and turbulent flow regimes. The laminar velocity profiles at the exit of the annular region are shown in figure 2(a). These profiles were found to be in agreement with the exact solution of a fully developed laminar annulus flow. The laminar-turbulent transition occurred when the Reynolds number was about 1600. The turbulent flow velocity distributions in figure 2(b) show that the flow could be regarded as a fully developed turbulent annulus flow for  $Re > 2000$ . The maximum turbulence levels of all the laminar cases were below 1% while in the turbulent flow regime the r.m.s. axial velocity fluctuations obviously increased and reached a maximum value of 12% in the neighbourhood of the boundary.

### 3. Results

#### 3.1. Flow pattern and reattachment length

Figure 3 shows a schematic drawing and a photograph of the corner recirculation zone downstream from the abrupt step. A primary recirculation zone and a secondary

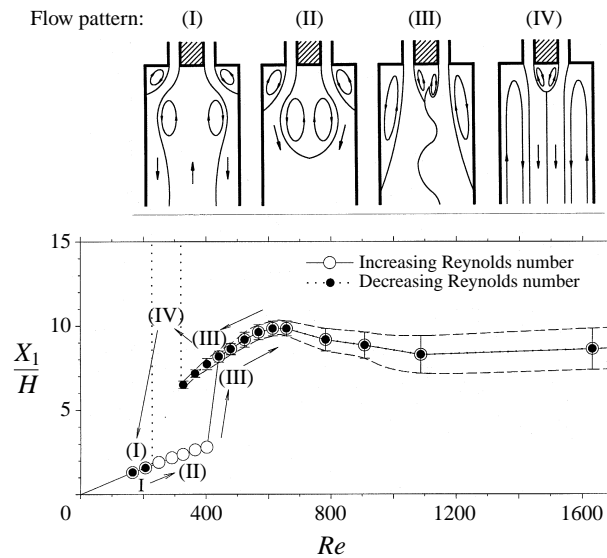


FIGURE 4. Regions of the characteristic flow modes in the primary reattachment length and the Reynolds number domains.

recirculation zone can be clearly distinguished in this picture; further, the lengths of the recirculation zones can be determined by observing the smoke streaks.

Based on the Reynolds number,  $Re$ , and the primary reattachment length,  $X_1$ , the flow field for an annular flow over an axisymmetric sudden expansion could be classified into four distinct flow regimes. The flow patterns of these flow regimes are called: (I) open annular flow, (II) closed annular flow, (III) vortex shedding, and (IV) stable central flow. Figure 4 shows the variations of  $X_1$  versus  $Re$ . A schematic drawing of the four flow patterns is also given in this figure. Figure 4 exhibits two different paths as the Reynolds number was either increased or decreased.

For the first path, as the Reynolds number was increased, the pattern of open annular flow (I) was observed when  $Re < 230$ . The sub-atmospheric pressure downstream of the sudden-expansion step was lower than that downstream of the centrebody; this caused the flow to expand radially and to reattach to the pipe wall over a short distance. Further, the velocity of the annular flow was low, and the sub-atmospheric pressure in the central core region behind the centrebody was not low enough to cause a reversal of the separation surface, which emanated from the edge of the centrebody. Consequently, a large central recirculation zone formed behind the centrebody, and the reversed flow in the central core extended through the whole pipe.

When the Reynolds number was increased to over 230, the sub-atmospheric pressure in the central core region was then lower than that in pattern (I) due to the increase of the annular flow velocity. The separation surface downstream thus moved toward the central axis. Finally, the central recirculation zone became closed, and this flow pattern is called closed annular flow. The primary reattachment length,  $X_1$ , was linearly proportional to the Reynolds number when  $Re < 440$ . For patterns (I) and (II), the primary reattachment points were observed to be very stable and fixed at a constant distance.

The flow pattern suddenly changed to pattern (III), vortex shedding, when the Reynolds number reached 440. Since the inertial momentum of the annular flow was high enough to overcome the sub-atmospheric pressure behind the abrupt ex-

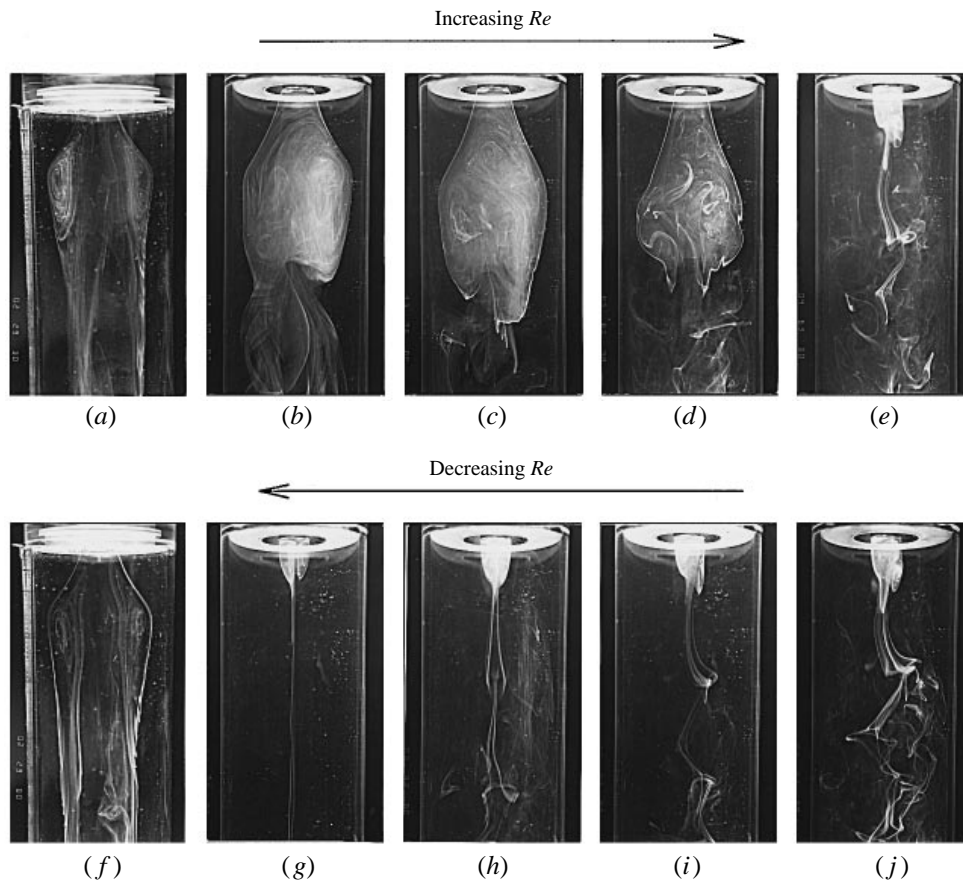


FIGURE 5. Photographs of flow patterns as the Reynolds number increased: (a)  $Re = 165$ , (b) 250, (c) 325, (d) 405 and (e) 480; as the Reynolds number decreased: (f)  $Re = 165$ , (g) 250, (h) 325, (i) 405 and (j) 480.

pansion step, the flow became less stable, and a small recirculation bubble behind the centrebody with vortex shedding was observed. The primary reattachment length increased abruptly when the Reynolds number reached 440. The corner recirculation zone was suddenly enlarged. Moreover, the flow in this regime became very unsteady. The corner recirculation zone fluctuated and the reattachment point was observed to move upstream and downstream. In figure 4, the ranges of the primary reattachment points are represented by the dashed lines, and the open circles for pattern (III) represent the mean values of the observed reattachment lengths. As the Reynolds number was further increased, the primary reattachment length reached a maximum value and then decreased slightly thereafter. This peak value was observed to be as large as 10 step heights and to occur when the Reynolds number was about 660. This flow pattern is very different from the first two and the shedding structure behind the centrebody played a dominant role in affecting the flow structure downstream. Visual photographs of flow patterns as the Reynolds number was increased are shown in figure 5(a) for open annular flow, figures 5(b), 5(c) and 5(d) for closed annular flow, and figure 5(e) for vortex shedding.

For the second path, where the Reynolds number was gradually decreased, the behaviour of the primary reattachment length, represented by the filled circles for

$X_1$ , was the same as when the Reynolds number was increased. However, the flow structure of vortex shedding was still observed when the Reynolds number was decreased to 325. When the Reynolds number was below 325, the pattern of vortex shedding could no longer be observed. Instead, a very stable central recirculation bubble behind the centrebody was formed. Part of the fluid on the separation surface was observed to be absorbed into the recirculation zone behind the centrebody, while other fluid moved downstream as shown by a fine smoke tail behind the recirculation bubble. The corner recirculation zone became infinitely long and extended to the exit of the pipe (1.2 m in length). This flow pattern is called stable central flow. As the Reynolds number was further reduced to 230, the same Reynolds number at which pattern (I) transformed into pattern (II) for increasing Reynolds number, the flow pattern changed from (IV), stable central flow, to (I), open annular-flow. On the second path as the Reynolds number was decreased, figures 5(j), 5(i) and 5(h) show the flow pattern of vortex-shedding, figure 5(g) shows the typical pattern of stable central flow, and figure 5(f) gives the flow pattern of open annular flow. In the vortex-shedding regime, the shedding process is featured by three-dimensional vortex line drawn through the central recirculation bubble, which convect downstream in loop-like structures. The whole picture of the shedding process is clearly illustrated in figure 5(h) or 5(i),  $Re = 325$  and  $Re = 405$ , respectively, and the non-dimensional shedding frequencies,  $fd/U_m$ , are about 0.23, where  $f$  is the measured shedding frequency.

From figures 4 and 5, it is interesting to note that there existed a hysteresis phenomenon for the variations of flow pattern as the Reynolds number was increased from 230 to 440 and then decreased back to 230. The occurrence of bifurcation for a confined annular flow stemmed from the hysteresis effect due to the interactions of the sub-atmospheric pressure between the two regions: downstream of the centrebody and downstream of the sudden-expansion step. This phenomenon resulted in three different flow patterns, as well as the variations of the reattachment length, for Reynolds numbers ranging from 230 to 440.

### 3.2. Mean velocities and velocity fluctuations

Detailed LDA measurements were carried out in various test sections and under different Reynolds number conditions. Figure 6 gives the LDA-measured mean axial velocity distributions for  $Re = 660$ . In this figure,  $U_o$  is the maximum axial mean velocity at the exit. Figure 7 shows the corresponding stream functions calculated from the measured velocities. As depicted in figure 7, the flow separated at the edges of the expansion step and the edges of the centrebody. Three recirculation regions can be clearly seen in this flow field: the central recirculation bubble formed immediately behind the centrebody, the primary corner recirculation zone formed behind the expansion step, and the secondary corner recirculation zone located between the wall of the step and the primary recirculation zone. The central recirculation bubble was found to be within  $0.38D_o$  downstream of the centrebody and within the radial position of diameter  $d$ . The results shown in figure 7 for the lengths of the primary and secondary recirculation zones are in agreement with those obtained using the flow visualization technique.

Figure 6 shows the development of the flow field along the axial direction from the expansion step. It can be seen that there was no flow reversal for  $x/D_o > 2.3$  ( $x/H > 9.3$ ) in the neighbourhood of the pipe wall. The maximum value of the axial velocity at each cross-section decreased slowly with the increasing axial distance for  $x/D_o < 1$  and then decreased rapidly for  $x/D_o > 1$ . The characteristics of the axial

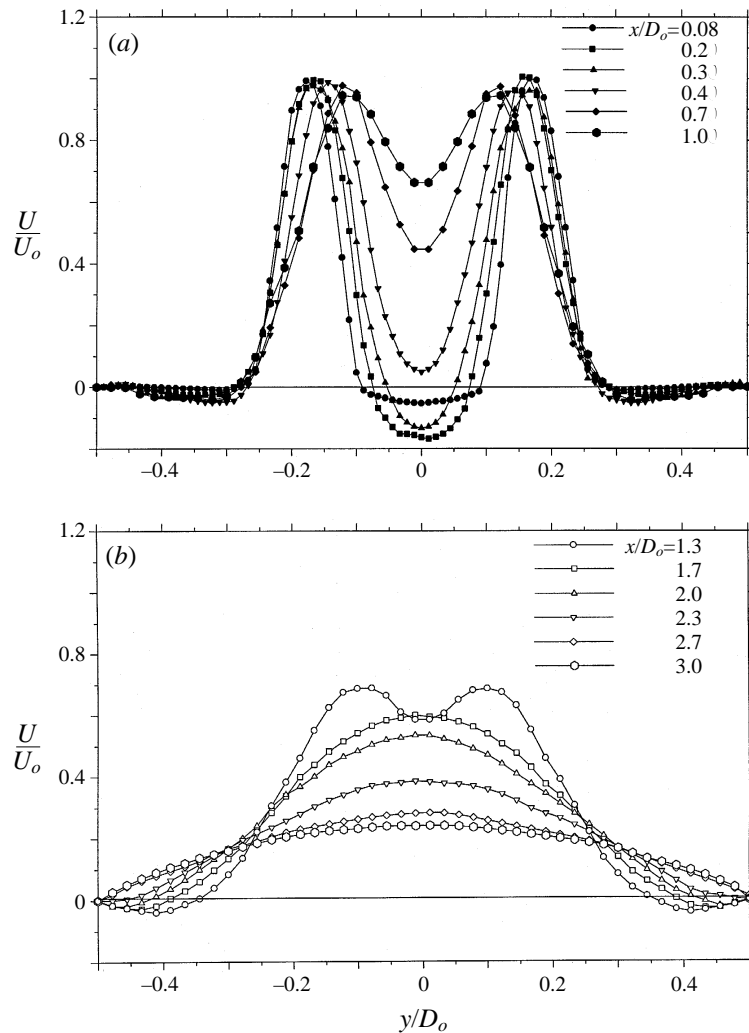


FIGURE 6. LDA-measured results for axial velocity profiles ( $Re = 660$ ). (a)  $x/D_o < 1$ ; (b)  $x/D_o > 1$ .

velocities downstream from the centrebody could be easily studied by examining the centreline development of the axial velocities,  $U_c$ , shown in figure 8. Downstream from the stagnation point, the centreline mean velocities increased rapidly with the downstream distance since the central flow was accelerated by the surrounding annular air stream, then reached a maximum value of  $0.7U_o$  at about  $x/D_o = 1$ , and finally decreased gradually for  $x/D_o > 1$  due to the expansion of the flow in the pipe. Furthermore, from figures 6 and 7, the annular flow at the exit section contracted slightly owing to the subatmospheric pressure behind the centrebody, then kept a nearly constant area from  $x/D_o = 0.4$  to  $x/D_o = 1$ , and finally spread laterally toward the pipe wall.

The normalized axial-component r.m.s. velocity fluctuations along the centreline,  $u'_c/U_o$ , increased rapidly with the axial distance (nearly as a power law) in the region inside the recirculation bubble, as shown in figure 8. This result indicates that the flow inside the recirculation bubble was quite unstable due to vortex shedding.

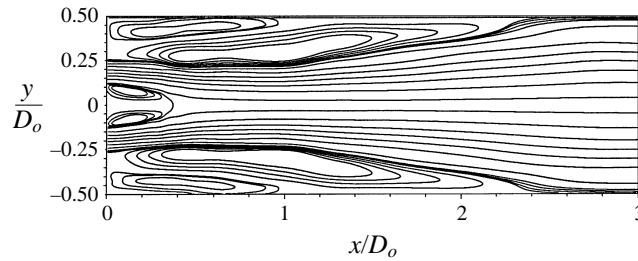


FIGURE 7. The results of the corresponding stream-function contours calculated from the measured velocities.

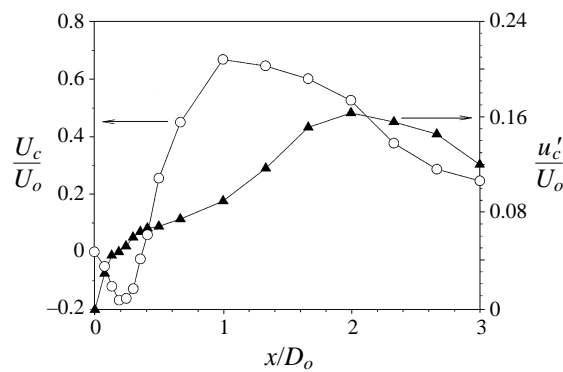


FIGURE 8. Mean axial velocities and r.m.s. velocity fluctuations along the centerline for  $Re = 660$ .

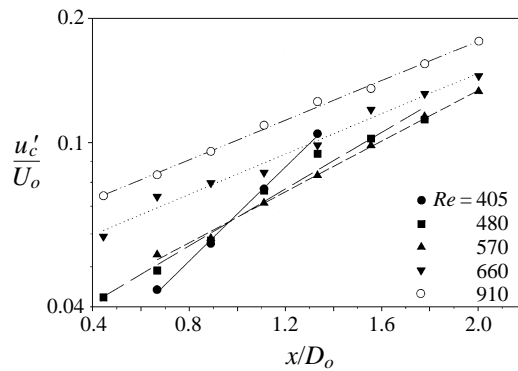


FIGURE 9. Spatial growth of velocity fluctuations along the centreline for flows with various Reynolds numbers.

Moreover, the r.m.s. velocity fluctuations grew nearly exponentially with the axial distance downstream the recirculation bubble, until a maximum value of  $0.16U_o$  was reached at  $x/D_o \approx 2$ , and then decayed gradually further downstream.

In figure 9, the normalized r.m.s. velocity fluctuations along the centreline are plotted against the axial positions,  $x/D_o$ , for various Reynolds numbers. The vertical axis was in a logarithmic scale, and the horizontal axis ranged from the apex of the recirculation bubble to the location of maximum velocity fluctuations. As shown in this figure, the spatial growth of the velocity fluctuations was almost exponential, and the slope of the growth decreased as the Reynolds number increased for  $Re \leq 660$ . Upon

further increase of Reynolds number beyond 660, the slope remained constant. The results for the growth of r.m.s. velocity fluctuations under various Reynolds number conditions indicate that the primary reattachment length increased as the Reynolds number increased from 325 and then reached a maximum value when  $Re = 660$ : that is, the decreasing slope of the growth of the velocity fluctuations led to an increase in the primary corner reattachment length. When  $Re > 660$ , the slope of the growth remained at a constant value, but the normalized r.m.s. velocity fluctuations along the axial direction increased as the Reynolds number increased. This result caused the primary reattachment length to gradually decrease for  $Re > 660$ .

In summary, for the flow in regime (III), the deterministic mechanism of flow reattachment was mainly due to the spatial growth of vortex shedding from the centrebody. These results provide more evidence to complement the observed strong influence of vortical structure behind the centrebody by flow visualization. This phenomenon is different from that reported by Back & Roschke (1972) for the case without the centrebody. In their case the flow was characterized by the growth of the undulating motion of the vortex-sheet-like shear layer between the central jet and the reverse flow for the corner recirculation zone. In the present study vortex shedding from the centrebody played a more important role than did shear-layer instability, which emanated from the edge of the sudden-expansion step. Moreover, this phenomenon can also explain why the primary reattachment lengths in regime (III) were significantly shorter than those reported by Macagno & Hung (1967) and Back & Roschke (1972) for the same expansion ratio ( $E = D_o/D$ ) of 2. The effects of vortex shedding for flow pattern (III) were so pronounced that the reattachment lengths were determined by the lateral extent of the undulating vortex shedding, which caused the flow to spread and extend laterally towards the pipe wall.

#### 4. Concluding remarks

In the present experimental investigation, the flow structures of an annular flow with a centrebody over an abrupt circular expansion have been classified into four different flow patterns. The complicated variations of the reattachment length with the Reynolds number clearly revealed that the hysteresis phenomenon of flow reattachment occurred between  $Re = 230$  and 440, and this range of Reynolds numbers was dependent on the length and the exit condition of the sudden-expansion pipe. The present results were obtained by fixing the length of the sudden-expansion pipe. The exit condition was carefully controlled to avoid the possible influence of the surrounding air. For a flow in the vortex-shedding regime, the flow field downstream the sudden expansion and the corresponding reattachment lengths were dominated by the vortex shedding behind the centrebody and the wake vortices downstream of it.

Further, two modes of the vortex shedding process were found in this experiment for the flow at higher Reynolds numbers: that is, the flow phenomenon behind the centrebody become more complicated as the Reynolds number was increased. The characteristics of these two modes of shedding and their frequency variations with  $Re$  need to be further investigated. A study on the shedding process as it varies with the Reynolds number and the downstream distance is in progress.

The present work was supported by the National Science Council of Taiwan under grants NSC85-2212-E002-012 and NSC86-2212-M002-022. The authors also would like to express their gratitude to Potters-Ballotini GmbH of Germany for their very

generous supply of glass beads, which were used as the seeding tracers for LDA measurements.

## REFERENCES

- ARMALY, B. F., DURST, F., PEREIRA, J. C. F. & SCHÖNUNG, B. 1983 Experimental and theoretical investigation of backward-facing step flow. *J. Fluid Mech.* **127**, 473–496.
- BACK, L. H. & ROSCHKE, E. J. 1972 Shear-layer flow regimes and wave instabilities and reattachment lengths downstream of an abrupt circular channel expansion. *Trans. ASME E: J. Appl. Mech.* **39**, 677–681.
- BADEKAS, D. & KNIGHT, D. D. 1992 Eddy correlations for laminar axisymmetric sudden expansion flows. *Trans. ASME I: J. Fluids Engng* **114**, 119–121.
- CHAN, W. T. & KO, N. W. M. 1978 Coherent structures in the outer mixing region of annular jets. *J. Fluid Mech.* **89**, 515–533.
- DURST, F., PEREIRA, J. C. F. & TROPEA, C. 1993 The plane symmetric sudden-expansion flow at low Reynolds numbers. *J. Fluid Mech.* **248**, 567–581.
- EATON, J. K. & JOHNSTON, J. P. 1981 A review of research on subsonic turbulent flow reattachment. *AIAA J.* **19**, 1093–1100.
- GOULD, R. D., STEVENSON, W. H. & THOMPSON, H. D. 1990 Investigation of turbulent transport in an axisymmetric sudden expansion. *AIAA J.* **28**, 276–283.
- KO, N. W. M. & CHAN, W. T. 1979 The inner regions of annular jets. *J. Fluid Mech.* **93**, 549–584.
- MACAGNO, E. O. & HUNG, T. K. 1967 Computational and experimental study of a captive annular eddy. *J. Fluid Mech.* **28**, 43–64.
- RESTIVO, A. & WHITELAW, J. H. 1978 Turbulence characteristics of the flow downstream of a symmetric, plane sudden expansion. *Trans. ASME I: J. Fluids Engng* **100**, 308–310.
- ROOS, F. W. & KEGELMAN, J. T. 1986 Control of coherent structures in reattaching laminar and turbulent shear layers. *AIAA J.* **24**, 1956–1963.